Journal of Marine Research, 62, 595–609, 2004

Variability of the biological front south of Africa from SeaWiFS and a coupled physical-biological model

by J. Llido[1], E. Machu[2], J. Sudre[1], I. Dadou[1] and V. Garçon[1]

ABSTRACT

The spatio-temporal variability of the biological front in the Agulhas Current system is investigated by comparing SeaWiFS chlorophyll *a* data and modeled chlorophyll fields over the October 1997–October 2001 period. The latter fields are simulated using a regional eddy-permitting (1/3° × 1/3°) coupled physical (AGAPE)-biological model forced by the monthly atmospheric NCEP/NCAR reanalysis. The annual cycle of the observed chlorophyll within the Agulhas Current system biogeochemical provinces is quite well reproduced by the model. The modeled phase of the seasonality in the SWSIG (South Western Subtropical Indian Gyre) is opposite to that of the SCZ (Subtropical Convergence Zone encompassing the Agulhas Front-AF, the Subtropical Front-STF and the Subantarctic Front-SAF), in agreement with observations. In the SWSIG, the switch from nitrates limitation to light control for the modeled phytoplankton growth shifts southward from winter to summer. In the SCZ, light availability modulates growth throughout the year.

The wavelet average variance of the SeaWiFS data is slightly underestimated by the modeled chlorophyll variance over the four-year period within the 36–45S and 15–45E domain. This might originate in the interannual monthly NCEP forcing which does not include the high frequency information of the atmospheric fluxes. The model coarse resolution precludes a proper simulation of vertical motions produced by submesoscale flows thereby underestimating biological variability. Interestingly, the modeled chlorophyll distribution mimicks the strong early retroflection of the Agulhas Current in summer 2001 which induces a southward displacement of the STF/SAF double front.

1. Introduction

The region (Fig. 1) is composed of the Agulhas Current proper (AC), flowing southward along the South African east coast (Lutjeharms, 1996; Lutjeharms *et al.,* 2003) which leaves the South African continental shelf and retroflects in a tight anticyclonic loop between 15E and 20E (Lutjeharms and van Ballegooyen, 1988). The Agulhas Return Current (ARC), as it emerges from the Agulhas Retroflection, flows eastward to the South Indian Ocean at around 39.5S (Lutjeharms and Ansorge, 2001) along the Subtropical Convergence (STC), with significant meandering caused by bottom topography and

1. LEGOS/CNRS/UPS/UMR556, 18 Av. E. Belin, 31401 Toulouse, Cedex 9, France. ***email: veronique.garcon@cnes.fr***

2. Department of Oceanography, University of Cape Town, R. W. James Building, Private Bag 7701 Rondebosch, South Africa.

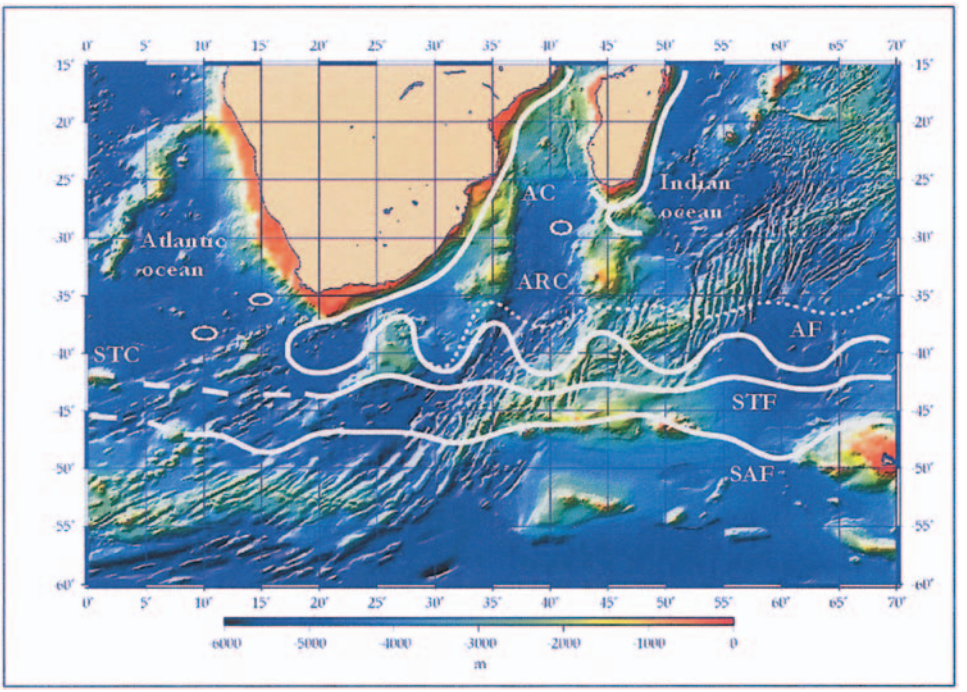

Figure 1. Schematic representation of the Agulhas Current System. Key bathymetric features are indicated. Also represented are the dynamical AF fronts between 35 and 45S in January 1998 (dotted line) and January 2000 (full line) in the model.

current instability (Quartly and Srokosz, 2002; Boebel *et al.,* 2003). The frontal system formed by the Agulhas Front (AF) in close juxtaposition with the Subtropical Front (STF), associated to the ARC and STC, respectively, and farther south by the Subantarctic Front (SAF) is a region of strong mesoscale variability (Matano *et al.,* 1998; Weeks *et al.,* 1998). It is characterized by recurrent eddies shedding their westward propagation and by the ARC meanders with nuanced interannual variability (Quartly and Srokosz, 2002; Boebel *et al.,* 2003). North–south meanders of the ARC have been described as a topographic Rossby wave by Harris and Bang (1974), and clearly identified around 38S with high chlorophyll pigment levels from the CZCS (Coastal Zone Color Scanner) signal by Weeks and Shillington (1994) and from SeaWiFS (Sea-viewing Wide Field-of-view Sensor) by Machu *et al.* (1999) and Machu and Garçon (2001). High chlorophyll pigment levels are observed in this juxtaposition of fronts, with a pronounced interannual variability (Weeks and Shillington, 1996; Moore and Abbott, 2000). Indeed, the AF seems to limit the spatial distribution of phytoplankton pigment northward, due to nutrient limitation in Subtropical Waters, whereas the STF frontal region is marked by distinctly elevated chlorophyll *a* concentrations with a maximum concentration when the AF, STF and SAF are in close proximity (Read *et al.,* 2000).

The purpose of this work is to examine the spatial and interannual variability of the Agulhas frontal system, through a comparative study between SeaWiFS and modeled chlorophyll fields. Section 2 will describe the data and the coupled physical-biological model used along with the wavelet analysis. The seasonal and interannual variability of the chlorophyll fields will be investigated in Section 3. Discussion of the findings follows in Section 4.

2. Data and methods

a. Data

A four-year long time series from October 1997 to September 2001 of ocean color data are used in this study. Phytoplankton pigment concentrations used are obtained from monthly SeaWiFS products of level 3 binned data, generated by the NASA Goddard Space Flight Center (GSFC) Distributed Active Archive Center (DAAC) with reprocessing 3 (version May 2000, Robinson *et al.,* 2000). The bins correspond to grid cells on a global grid, with each cell approximately 9 by 9 km.

b. Coupled model

A three-dimensional regional physical model AGAPE (AGulhas As Primitive Equation, Biastoch and Krauss, 1999) coupled with a biological model (Nutrient, Phytoplankton, Zooplankton, Detritus) is used. The AGAPE model consists of a set of primitive equations, where the horizontal velocity components and tracers are prognostically integrated while the vertical velocity component is diagnosed from the continuity equation. The model covers the South Indian and Atlantic oceans from 6.5S to 65S and 60W to 115E. The horizontal resolution is eddy-permitting with $1/3^\circ \times 1/3^\circ$ in the region of interest (20W–70E). The water column is resolved with 29 levels on the vertical with a Δz varying from 15 (upper ocean) to 250 m (at depth). The bottom topography is based on the NGDC (National Geophysical Data Center) 5 arc minute dataset and smoothed by a two-dimensional symmetric filter (Shapiro, 1970) once in the fine-resolution region and three times in the rest of the model domain.

Horizontal subgrid-scale diffusion and viscosity are parameterized using a biharmonic operator. In the vertical, a constant Laplacian parameterization is used. A simple mixed layer model of the Krauss-Turner type is used (Krauss and Turner, 1967; wind-driven part only). More information about the dynamical model and treatment of open boundaries can be found in Biastoch and Krauss (1999) and Machu *et al.* (2004).

The model framework for the plankton dynamics is a classical N-P-Z-D nitrogen-based biological model developed by Oschlies and Garçon (1998, 1999). Processes within the trophic chain include phytoplankton growth and mortality, zooplankton growth by grazing on phytoplankton, excretion and mortality, and remineralization and sinking of detrital material, with uniform biological parameters for the entire domain.

Following Hurtt and Armstrong (1996), the phytoplankton growth rate is taken to be the

minimum of light- and nutrient-limited growth. Standing stocks and fluxes are computed in nitrogen units. Surface chlorophyll is not a prognostic variable but is diagnosed from the model state. Following Hurtt and Armstrong (1996), a chlorophyll-to-nitrogen ratio is used to convert modeled phytoplankton in nitrogen units to phytoplankton observed in chlorophyll units by

$$Chl = 1.59 \cdot \chi \cdot P$$

where P is phytoplankton nitrogen in mmolN/m^3 and Chl is in mg Chl/m^3, 1.59 corresponding to the standard chlorophyll to nitrogen ratio. If growth is light limited, then Chl:N = 1.59. χ_{max} which means Chl:N is maximum. We chose $\chi_{max} = 1$ which gives a C:Chl$_{min}$ = 50. If phytoplankton is nutrient limited, we adjust χ downward to make it equally limited by light and nutrients. We neglect the effect of χ on the light profile and then the growth rate limited by light is a linear function of χ. Therefore, χ is simply given by χ = nutrient limited growth rate/light limited growth rate. In this study, we fix an upper limit for the C:Chl equal to 120. The model does not take into account possible co-limitations by iron and/or silica.

Advection of the ecosystem components is modeled with a higher-order positive definite scheme (Oschlies and Garçon, 1998, 1999; Machu *et al.,* 2004).

We use monthly means of the NCEP/NCAR reanalysis over the 1995–2001 period (http://www.cdc.noaa.gov/cdc/reanalysis) for the atmospheric forcing of our coupled model. The surface salinity is restored on a 50-day time scale to the Levitus *et al.* (1994) climatology. For the interannual run, the surface temperature is restored on a 50-day time scale to the monthly means of SST from Reynolds *et al.* (2002). A direct penetrative insolation characterizes the shortwave radiation.

Initial conditions for all variables, physical as well as biological, in the coupled interannual simulation forced with the NCEP/NCAR reanalysis are the coupled model states from a climatological run performed by Machu *et al.* (2004). In the latter, the coupled model is forced by the ECMWF monthly climatology from Barnier *et al.* (1995). The model analysis phase with the NCEP/NCAR reanalysis is chosen to start in October 1997 allowing thirty three months of spin-up time after initialization in January 1995 with the fields of the climatological run. Values of parameters are those selected in Machu *et al.* (2004).

As for heat and salt, nitrate, phytoplankton, zooplankton and detritus are transported out of the domain using a radiation condition plus advection if the normal component of the velocity at the boundary is directed outward. For those boundary points where the normal velocity is into the domain, restoring of nitrate to the climatology of Conkright *et al.* (1994) and of phytoplankton, zooplankton and detritus to their initial profiles occurs.

c. Wavelet analysis

A 1D wavelet and power Hovmöller analysis (Machu *et al.,* 1999; Machu and Garçon, 2001) is conducted on the four-year (October 1997–September 2001) time series on both

SeaWiFS and modeled chlorophyll fields in the Agulhas Current system between 15E–45E and 36S to 45S to examine the spatio-temporal variability of the biological front.

Let's summarize the wavelet analysis as follows. Let x_n denote a signal that varies with equal spacing δx along an x-axis (it will follow a latitude circle) and $n = 0, \ldots$ N-1 longitude points. We chose a wavelet function $\Psi_0(\eta)$ (mother wavelet) that depends on a nondimensional distance parameter η. To be admissible as a wavelet, this function must have a zero mean, have a Fourier Transform that exists, and be localized in both distance and frequency space (Farge, 1992). An example is the Morlet wavelet, that we chose here, consisting of a plane wave modulated by a Gaussian:

$$\Psi_0(\eta) = \Pi^{-1/4}\, e^{i\omega_o \eta}\, e^{-\eta^2/2}.$$

The continuous wavelet transform of a discrete sequence, x_n, is defined as the convolution of x_n with a scaled and translated version of $\Psi_0(\eta)$:

$$W_n(s) = \sum_{n'=0}^{N-1} x_{n'}\, \Psi^* \left[\frac{(n' - n)\, \delta x}{s} \right]$$

where the (*) denotes the complex conjugate. If one varies the wavelet scale s (scale dilation parameter) and translates along the localized distance index n (translation parameter), one can construct a picture showing both the amplitude of any features versus the scale and how this amplitude varies with distance. Since the Morlet wavelet is complex, the wavelet transform is also complex. The local wavelet power spectrum is defined as the square of the modulus of the wavelet coefficients $|W_n(s)|$ (Torrence and Compo, 1998). It is usually normalized to have unit energy.

The extraction of the wavelet coefficient maxima from the local wavelet power spectrum gave us the range of wavelengths (380–760 km) associated to the meanders of the ARC and STC in a one-year SeaWiFS chlorophyll signal (Machu and Garçon, 2001) in the selected longitude domain (15–45E). One can then define the scale-averaged wavelet power as the weighted sum of the wavelet power spectrum over scales 380 to 760 km. At each latitude, the scale-averaged wavelet power over this 380–760 km band is computed according to:

$$\overline{W_n^2} = \frac{\delta_j \delta_x}{C_\delta} \sum_{j=j1}^{j2} \frac{|Wn(sj)|^2}{sj}$$

where δ_j is the spacing between discrete scales and the factor C_δ comes from the reconstruction of a δ-function from its wavelet transform using the function $\Psi_0(\eta)$ (Torrence and Compo, 1998). We thus obtain a two-dimensional longitude-latitude diagram power Hovmöller of the wavelet variance for chlorophyll for each month. The average of the power Hovmöller over all latitudes (between 36 and 45S) and longitudes

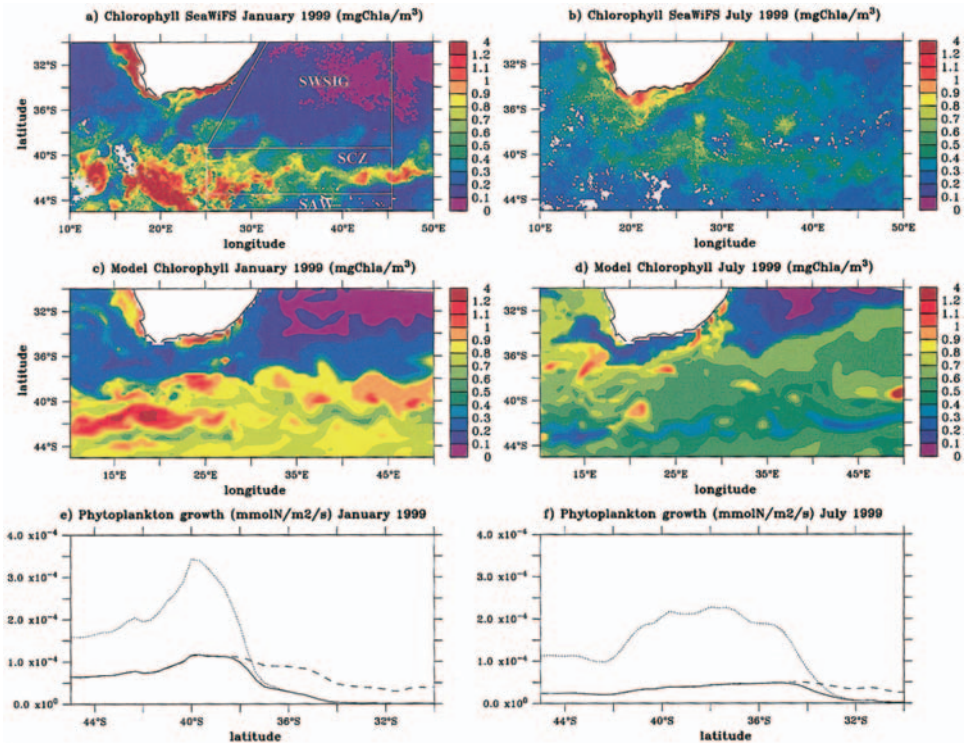

Figure 2. (a) January 1999 monthly composite of SeaWiFS chlorophyll concentrations (mg Chl/m^3). SWSIG, SCZ and SAW denote the South Western Subtropical Indian Gyre, the Subtropical Convergence Zone, and the Subantarctic Waters, respectively. (b) July 1999 monthly scene of SeaWiFS chlorophyll concentrations (mg Chl/m^3), (c) January 1999 monthly mean chlorophyll concentrations simulated by the coupled AGAPE and biological model for the first layer (7.5 m), (d) July 1999 monthly mean chlorophyll concentrations simulated by the coupled AGAPE and biological model for the first layer (7.5 m), (e) Evolution of the phytoplankton growth (either light or nutrient limited) (mmolN/m^2/s) averaged from 35 to 45E and integrated over the two upper layers (32.68 m) of the model, in January 1999: full line: phytoplankton growth, dotted line: nutrient limited growth and dashed line: light-limited growth. (f) Same as in (e) for July 1999.

(15–45E) then gives a measure of the global 380–760 km variance for the chlorophyll signal as a function of time.

3. Variability of chlorophyll fields

a. Seasonal variability

Let us first present the three distinct biogeochemical provinces of the Agulhas Current system as measured by SeaWiFS (Fig. 2a,b): the South Western Subtropical Indian Gyre (SWSIG), the Subtropical Convergence Zone (SCZ) encompassing the AF, STF and SAF frontal system and south of it, the Subantarctic Waters (SAW) (Machu *et al.,* 2004).

The SWSIG area is characterized by very low chlorophyll content (up to 0.2 mg Chl/m^3) in summer 1999 (Fig. 2a) whereas in winter 1999 (Fig. 2b) typical concentrations range between 0.2 to 0.6 mg Chl/m^3. The southern boundary of the SWSIG along 39S exhibits higher chlorophyll content (up to 0.8 mg Chl/m^3). The SCZ is distinguishable by its very high chlorophyll levels, up to 4 mg Chl/m^3 in localized patches, in the monthly January 1999 scene. Crests and troughs of the Rossby wave meanders appear clearly (Fig. 2a). In contrast, the monthly July 1999 scene presents a diffuse AF, and lower concentrations (0.3–0.6 mg Chl/m^3) in the frontal system (Fig. 2b). South of the SCZ in the SAW, in both scenes, surface chlorophyll concentrations stay around 0.1–0.4 mg Chl/m^3. In the northwestern area of the SAW however, chlorophyll concentrations can reach higher values (up to 1.1 mg Chl/m^3) in summer 1999 due to the vicinity of the Agulhas retroflection.

Let us examine the surface chlorophyll distribution as simulated by the coupled model for these two January and July 1999 scenes. The subtropical biogeochemical province is quite well reproduced in summer, chlorophyll concentrations being slightly higher by 0.1–0.2 mg Chl/m^3 than SeaWiFS data, in particular in the southern boundary of the SWSIG (Fig. 2c). Phytoplankton growth is limited by nitrates in the model until around 38S then a switch to light limitation occurs (Fig. 2e). In winter, modeled chlorophyll concentrations fall within the same range as in SeaWiFS data but the northern low chlorophyll values visible in SeaWiFS data extend too far south (36S) in the model (Fig. 2d). In the SWSIG northern part, nutrients limit growth in the model but south of 34S, light availability modulates phytoplankton growth (Fig. 2f).

The northern limit of the modeled SCZ describes a meandering Rossby wave on the January 1999 scene (Fig. 2c). One can note a weak inclination eastward of 30E toward the north of this northern limit as compared with the SeaWiFS observations (Fig. 2a,c). Simulated chlorophyll concentrations come close to SeaWiFS values but the spatial distribution differs somehow. The SeaWiFS enhanced values appear as a multitude of localized patches whereas the model fields show large areas of high chlorophyll values (0.8 to 1.1 mg Chl/m^3). Within the SCZ, light in the model always plays the limiting role to growth (Fig. 2e,f). South of the SAF, *in situ* silicate and/or iron limitation would limit biomass development in this HNLC (High Nutrient Low Chlorophyll) region which is not the case in our model, resulting in a higher biomass than the observed one (Fig. 2c,d).

To study the seasonality, we examine the time series of chlorophyll data along 37S (in the SWSIG) and 41S (in the SCZ) (Fig. 3). At 37S, a distinct annual cycle is observed in SeaWiFS chlorophyll (Fig. 3a) between 15E–45E with minimal concentrations in summer and maxima in winter-spring. The annual mean, amplitude and phase associated to this observed seasonal cycle are equal to 0.35 mg Chl/m^3, 0.13 mg Chl/m^3 and 10 months, respectively. Modeled chlorophyll fields (Fig. 3b) reproduce reasonably well this annual cycle with maximal concentrations in spring and minima in summer and fall. Note, however, that the minimal concentrations in the model are not as well marked as in SeaWiFS. The annual amplitude and phase of modeled chlorophyll fields between 15E–45E along 37S are close to those determined with SeaWiFS data, 0.15 mg Chl/m^3 and

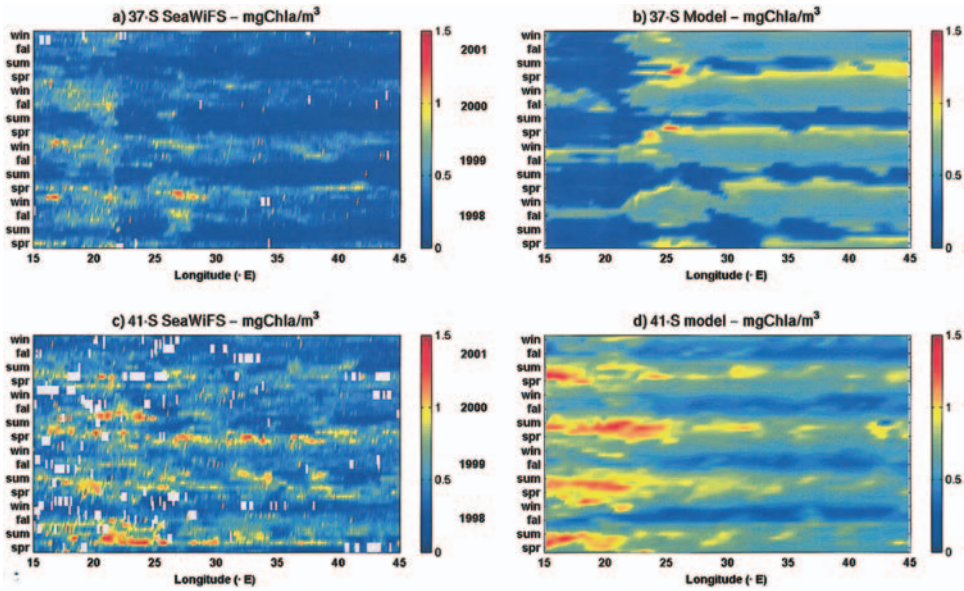

Figure 3. Time-longitude diagrams of chlorophyll concentrations (mg Chl/m^3) at 37S for SeaWiFS (a) and for model outputs (b), at 41S for SeaWiFS (c) and for model outputs (d).

11 months, respectively, whereas the annual mean value, 0.52 mg Chl/m^3, is slightly higher than the SeaWiFS annual mean.

In the SCZ, along 41S (Fig. 3c,d), the annual cycle is characterized by high (low) chlorophyll levels in spring–summer (fall–winter), both in SeaWiFS and modeled chlorophyll. The seasonal variability, observed with SeaWiFS data within the frontal system, emerges also in the modeled chlorophyll fields. The phase of the annual cycle is similar in data and model outputs (3 months) whereas the annual mean and amplitude are higher in the model (0.65 and 0.2 mg Chl/m^3, respectively) than in SeaWiFS data (0.51 and 0.12 mg Chl/m^3, respectively).

b. Interannual variability of the chlorophyll distributions

Figure 4 shows the wavelet average variance (between 15E–45E) over all latitudes within 36 to 45S over the four-year time series for SeaWiFS and modeled Chl *a.* The wavelet variances are normalized by the maximum variance achieved over this October 1997–October 2001 time period for both chlorophyll signals.

The modeled chlorophyll variance generally underestimates slightly the SeaWiFS variance (Fig. 4). In July–August, the two variance curves come close to each other; in fall and winter they present the lowest values (down to 0.01). The seasonal variability emerges unambiguously both in the observations and the model variances with the maximal values in spring–summer. In 2000, both modeled and SeaWiFS chlorophyll show the highest

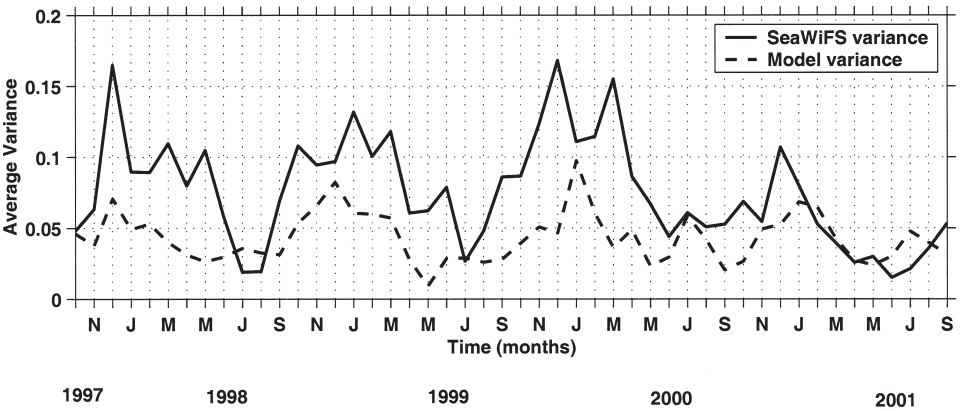

Figure 4. Wavelet average variance, in the 15–45E longitude band, for chlorophyll data as a function of time resulting from an average over all latitudes (36 to 45S) of the two-dimensional power Hovmöller. Full lines indicate SeaWiFS data whereas dashed lines indicate modeled chlorophyll data.

wavelet variances (up to 0.1 and 0.17, respectively). In 2001, both variance values are similar due to a weaker variance of observations than in previous years (Fig. 4).

The behavior of the modeled chlorophyll field at 37S (Fig. 3b, and also at 36S, not shown here) changes somehow over time. On years 1998 and 1999, between 27–33E, very low modeled chlorophyll concentrations exist which then disappear in later years. This can be explained by a northward inclination of the simulated front eastward of 30E in years 1998–1999 as compared with a modeled zonal front in years 2000–2001 (Fig. 1). The modeled isotherms are superimposed on the simulated chlorophyll distribution in Figure 5a,b. Following Read *et al.* (2000), the 10.5°C isotherm is chosen to tentatively characterize the SAF, the 14.5°C isotherm the STF, and the 18.5°C isotherm the AF. One can see an intrusion of colder-than-usual waters eastward of 30E in the model, simultaneously with a front inclination (Fig. 5a,b). This phenomenon is directly linked to the 1998–1999 forcing used, the NCEP/NCAR shortwave flux and the Reynolds SST being much weaker than in years 2000–2001 in this area, which results in a much lower phytoplankton growth. This northward shift of the dynamical AF front in summer 1998 therefore affects the chlorophyll distribution (Fig. 5a,c). The biological front, with chlorophyll values of 0.7–0.8 mg Chl*a*/m^3, is shifted northward from around 40S to 36S eastward of 30E. A tongue of low primary production ($\leq$5 gC/m^2/season), penetrating as south as 38S at 30E, accompanies the northward shift in 1998 (Fig. 5c). The highest chlorophyll concentration values are found north of the STF (Fig. 5a).

In summer 2000, high chlorophyll concentrations (0.8–0.9 mg Chl/m^3) meander around 38–39S yielding a zonal front structure and exhibiting a well defined ARC Rossby wave (Fig. 5b). Simulated enriched chlorophyll large patches are localized on either side of the STF in summer 2000 (Fig. 5b) associated with a patchy grazing pressure while the highest

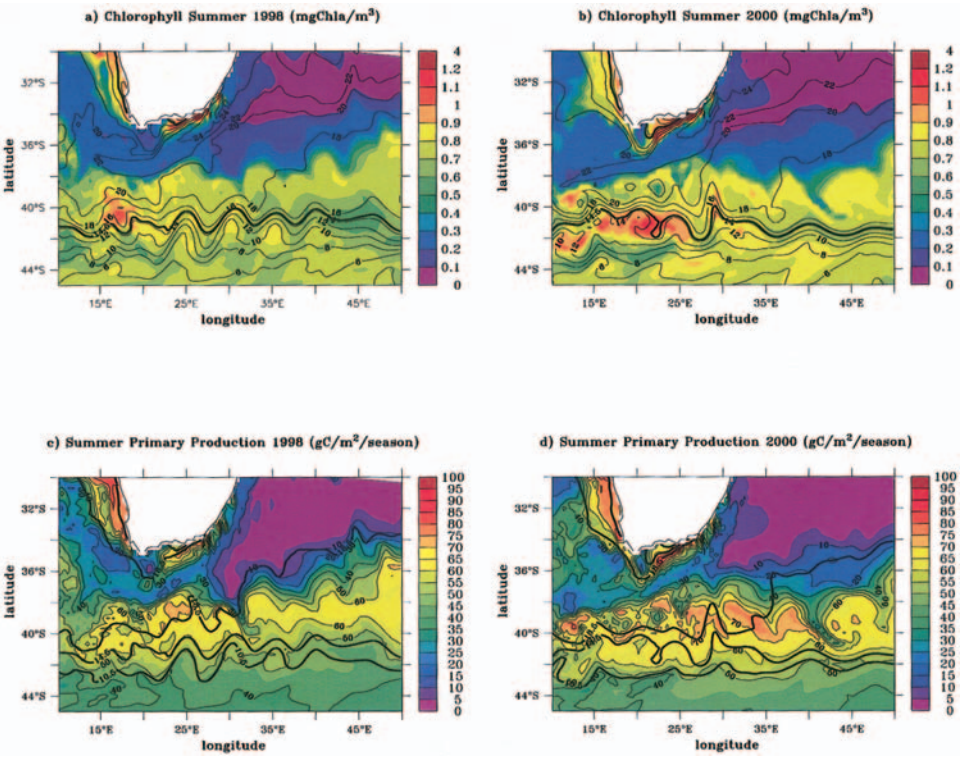

Figure 5. Summer chlorophyll concentrations (mg Chl/m^3) simulated by the model for the first layer (7.5 m) in 1998 (a) and 2000 (b). Black full contours indicate the isotherms (every 2°C), the bold black line indicates the 14.5°C isotherm. Summer modeled primary production integrated from 0 to 65 m, in gC/m^2/season, in 1998 (c) and 2000 (d). The 10.5°, 14.5° and 18.5°C isotherms are indicated by bold black lines and highlight the Subantarctic (SAF), Subtropical (STF) and Agulhas Front (AF), respectively, following Read *et al.* (2000).

values of the modeled primary production (75–80 gC/m^2/season) are simulated north of the STF (Fig. 5d). Indeed at this latitude, chlorophyll is present down to 60 m and the integrated primary production is high. Farther south, chlorophyll is restricted to shallower depths (30 m) and the primary production exhibits lower integrated values.

In the model, the AF-STF and SAF frontal system is displaced farther south in summer 2001 as compared with the previous years (Fig. 6). Examining closely the vertical structure between 20–25E, the STF (SAF) lies close to 41S (44S) in 2001 whereas these two fronts lie farther north in other years. Modeled concentrations of chlorophyll *a* peak when the modeled AF-STF and SAF are in close proximity in summers 1999 and 2000 (Fig. 6b,c). These combined front structures have a marked vertical stability and light levels are high within the shallow stable layer (≈30–40 m, Fig. 6b,c). The 2001 southward displacement seems to influence the modeled summer chlorophyll distributions. The latter exhibits a

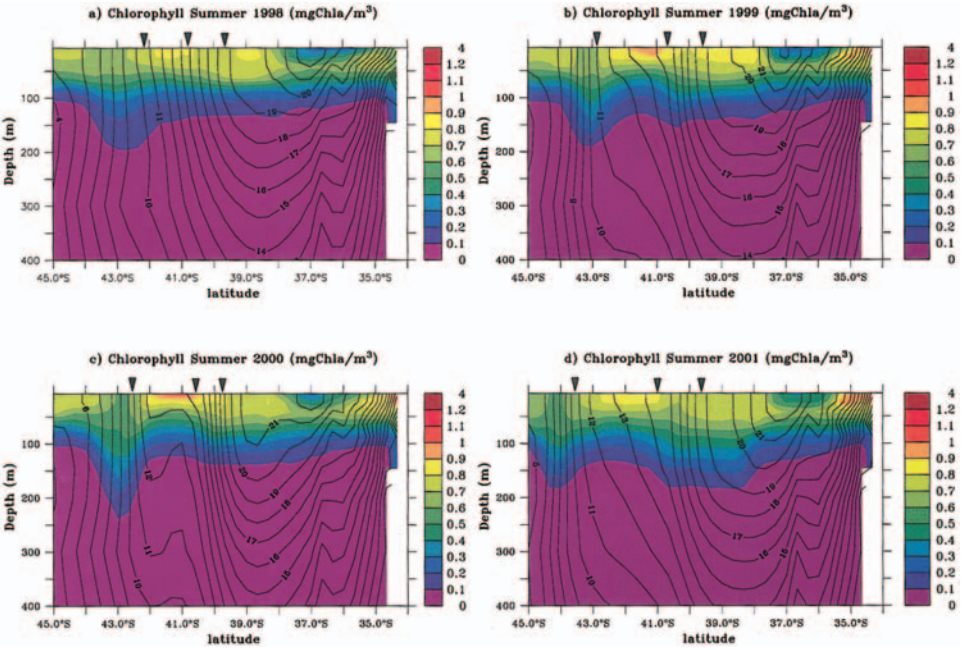

Figure 6. Vertical sections along a 20–25E average for chlorophyll *a* (mg Chl/m^3) in summer (a) 1998, (b) 1999, (c) 2000, and (d) 2001. Black lines represent isotherms. Reversed triangles indicate from north to south the outcrops of the 18.5°C, 14.5°C and 10.5°C isotherms.

large area of high chlorophyll values of 0.9 mg Chl/m^3, between the STF and SAF (41–43S) (Fig. 6d), farther south than in previous summers. Similarly, the associated deepening of the 0.1 mg Ch/m^3 isocontour of chlorophyll concentration is shifted southward in 2001, occurring between 44–45S.

4. Discussion

The primary objective of this study was to examine the spatio-temporal variability of the biological front in the Agulhas Current system comparing SeaWiFS and modeled chlorophyll fields produced by a regional eddy-permitting coupled physical-biological model forced by the monthly atmospheric NCEP reanalysis over the October 1997–October 2001 period.

In general, the annual cycle of the observed chlorophyll within the Agulhas Current system biogeochemical provinces is quite well reproduced by the model. The phases within the SWSIG and SCZ of the annual cycle of SeaWiFS and modeled chlorophylls coincide. However, the annual mean and amplitude of the modeled fields are slightly higher.

One must recall that the modeled chlorophyll fields within the SWSIG (at 37S) differ

from the SeaWiFS fields in certain years due to a northward shift of the modeled AF front. Indeed the interannual monthly NCEP forcing does not allow simulation of a zonal biological front, in disagreement with observations. Although the NCEP reanalysis does of course include interannual variations absent in the case of a climatological atmospheric forcing, one cannot affirm that the reanalysis provides realistic fluxes. Whether the 1998 and 1999 features in the NCEP/NCAR and Reynolds SST are real is very difficult to assert. They might not be since the simulated frontal shift is not present in the observations.

Both wavelet variance of modeled and SeaWiFS chlorophyll signals exhibit the same seasonal cycle, but modeled chlorophyll results exhibit lower variance levels than those obtained with SeaWiFS chlorophyll data. This may result from several causes. The interannual NCEP/NCAR forcing we use consists of monthly fields of wind stress, shortwave radiation and thus does not include the high frequency information of these atmospheric variables. Secondly, the model, with a coarse 1/3° horizontal resolution, cannot properly simulate vertical motions produced by submesoscale flows thereby underestimating biological variability (Flierl and McGillicuddy, 2002). This underestimation of variance is less severe in winter when biological activity is the weakest. These are the two main sources of underestimation on the modeling side. The spatial change in cloud cover over a month yields a spatial change in clear pixels on the daily SeaWiFS images. The monthly composites based on these images include this intrinsic source of variability. Another source of variability on the daily images is the presence of the sporadic bloom event features within the frontal system. These two effects are specific to the observations and might explain another part of the underestimation of the variance in our interannual simulation.

Interestingly, the model shows a significant change in the behavior of the system in year 2001 in agreement with observations. A low wavelet variance of SeaWiFS chlorophyll data characterizes the year 2001 (Fig. 4). A retroflection of the AC occurring farther to the east was present in summer 2001 (Quartly and Srokosz, 2002; Rouault and Lutjeharms, 2003). These authors, using SST observations from the TRMM Microwave Imager, noticed a change in the behavior of the Agulhas retroflection from October 2000 until March 2001. Usually an early retroflection induces a more southerly direction and southward penetration of the AC (Quartly and Srokosz, 1993). The SCZ is displaced farther south in the model. Indeed, considerable interannual variability is observed on the modeled position anomaly of the core Agulhas retroflection (furthest westward penetration of 22°C Agulhas water, as defined in Weeks and Shillington, 1996; Fig. 7). The October 2000–March 2001 period stands out as a peculiar period, the model mimicking well an AC retroflection being blocked farther to the east (Fig. 7).

One may question whether the observed interannual variability evident in both the position of the Agulhas retroflection and the extent of the Rossby wave in the Agulhas Current system may be related, with some delayed effect, to the Indian Ocean Dipole/El Niño events of 1997/1998. Indeed Schouten *et al.* (2002) showed that an oceanic teleconnection, through a sequence of Kelvin and Rossby waves, seems to exist between

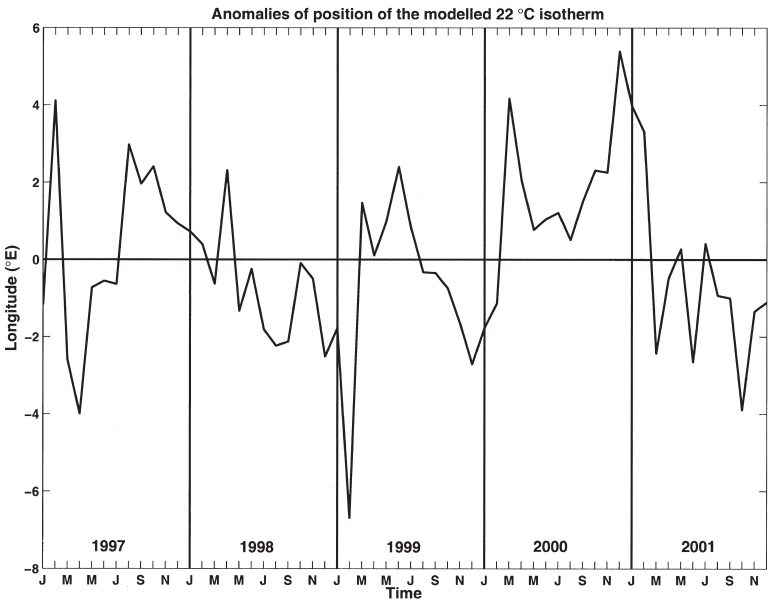

Figure 7. Anomalies of position of the modeled 22°C isotherm (anomalies around the 1997–2001 mean position). Positive anomaly is eastward of the mean position.

the equatorial winds in the Indian Ocean and the Agulhas system variability. During the 1997/1998 Indian Ocean Dipole (Saji *et al.,* 1999), strong easterlies prevailed over the Indian Ocean equatorial basin inhibiting the Kelvin wave signal to reach the coast of Indonesia. Consequently, no westward propagating Rossby waves were induced along 10–12S, a reduced eddy formation occurred on reaching the Madagascar and Mozambique Channel regions and a subsequent change resulted a couple of years later in the behavior of the Agulhas retroflection (Schouten *et al.,* 2002). How the disturbances of this propagating signal impact the distribution of a marine biomass proxy such as chlorophyll *a* is the subject of ongoing work.

Acknowledgments. This study was supported through CNES funding to LEGOS. J.L. particularly thanks J. Lutjeharms and M. Rouault for fruitful discussions during his two-month stay at the Department of Oceanography at Cape Town. NCEP reanalysis data were provided by the NOAA-CIRES Climate Diagnostics Center, Boulder, Colorado, USA from http://www.cdc.noaa.gov. Reynolds SST were obtained from http://www.emc.ncep.noaa.gov/research/cmb/sst_analysis. Wavelet software was provided by C. Torrence and G. Compo and is available at URL:// paos.colorado.edu/research/wavelets. We would like to thank the reviewers for their very fruitful and constructive comments on this manuscript.

REFERENCES

Barnier, B., L. Siefridt and P. Marchesiello. 1995. Thermal forcing for a global ocean circulation model from a three-year climatology of ECMWF analysis. J. Mar. Sys., *6,* 363–380.

Biastoch, A. and W. Krauss. 1999. The role of mesoscale eddies in the source regions of the Agulhas Current. J. Phys. Oceanogr., *29,* 2303–2317.

Boebel, O., T. Rossby, J. R. E. Lutjeharms, W. Zenk and C. Barron. 2003. Path and variability of the Agulhas Return Current. Deep-Sea Res. II, *50,* 35–56.

Conkright, M. E., S. Levitus and T. P. Boyer. 1994. Nutrients. World Ocean Atlas 1994, NOAA Atlas NESDIS, *1,* 99 pp.

Farge, M. 1992. Wavelet transform and their application to turbulence. Ann. Rev. Fluid. Mech., *24,* 395–457.

Flierl, G. and D. J. McGillicuddy. 2002. Mesoscale and submesoscale physical-biological interactions, *in* The Sea, *12,* A. R. Robinson, J. J. McCarthy and B. J. Rothschild, eds., Wiley and Sons, NY, 113–185.

Harris, T. F. W. and N. D. Bang. 1974. Topographic Rossby waves in the Agulhas Current. S. Afr. J. Sci., *70,* 212–214.

Hurtt, G. C. and R. A. Armstrong. 1996. A pelagic ecosystem model calibrated with BATS data. Deep-Sea Res. II, *43,* 653–683.

Krauss, E. B. and J. S. Turner. 1967. A one-dimensional model of the seasonal thermocline. II: The general theory and its consequences. Tellus, *19,* 98–105.

Levitus, S., R. Burgett and T. P. Boyer. 1994. Salinity. World Ocean Atlas 1994, NOAA Atlas NESDIS, *3,* 99 pp.

Lutjeharms, J. R. E. 1996. The exchange of water between the South Indian and South Atlantic Oceans: A review, *in* The South Atlantic Present and Past Circulation, G. Wefer, ed., Elsevier, 125–162.

Lutjeharms, J. R. E. and I. J. Ansorge. 2001. The Agulhas Return Current. J. Mar. Sys., *30,* 115–138.

Lutjeharms, J. R. E., O. Boebel and H. T. Rossby. 2003. Agulhas cyclones. Deep-Sea Res. II, *50,* 13–34.

Lutjeharms, J. R. E. and R. C. van Ballegooyen. 1988. The retroflection of the Agulhas Current. J. Phys. Oceanogr., *18,* 1570–1583.

Machu, E., A. Biastoch, A. Oschlies, M. Kawamiya, J. R. E. Lutjeharms and V. Garçon. 2004. Phytoplankton distribution in the Agulhas system from a coupled physical-biological model. Deep-Sea Res. I, (submitted).

Machu, E., B. Ferret and V. Garçon. 1999. Phytoplankton pigment distribution from SeaWiFS data in the subtropical convergence zone south of Africa: a wavelet analysis. Geophys. Res. Lett., *26,* 1469–1472.

Machu, E. and V. Garçon. 2001. Phytoplankton seasonal distribution from SeaWiFS data in the Agulhas Current system. J. Mar. Res., *59,* 795–812.

Matano, R. P., C. G. Simionato, W. P. M. de Ruijter, P. J. van Leeuven, P. T. Strub, D. B. Chelton and M. G. Schlax. 1998. Seasonal variability in the Agulhas retroflection region. Geophys. Res. Lett., *25,* 4361–4364.

Moore, J. K. and M. R. Abbott. 2000. Phytoplankton chlorophyll distributions and primary production in the Southern Ocean. J. Geophys. Res., *105,* (C12), 28709–28722.

Oschlies, A. and V. Garçon. 1998. Eddy-induced enhancement of primary production in a model of the North Atlantic Ocean. Nature, *394,* 266–269.

—— 1999. An eddy permitting coupled physical-biological model of the North Atlantic. 1. Sensitivity to advection numerics and mixed layer physics. Global Biogeochem. Cycles, *13,* 135–160.

Quartly, G. D. and M. A. Srokosz. 1993. Seasonal variation in the region of the Agulhas retroflection: studies with Geosat and FRAM. J. Phys. Oceanogr., *23,* 2107–2124.

—— 2002. SST Observations of the Agulhas and East Madagascar Retroflections by the TRMM Microwave Imager. J. Phys. Oceanogr., *32,* 1585–1592.

Read, J. F., M. I. Lucas, S. E. Holley and R. T. Pollard. 2000. Phytoplankton, nutrients and hydrography in the frontal zone between the Southwest Indian Subtropical gyre and the Southern Ocean. Deep-Sea Res. I, *47,* 2341–2368.

Reynolds, R. W., N. A. Rayner, T. M. Smith, D. C. Stokes and W. Wang. 2002. An improved *in situ* and satellite SST analysis for climate. J. Climate, *15,* 1609–1625.

Robinson, W. D., G. M. Schmidt, C. R. McClain and P. J. Werdell. 2000. Changes made in the operational SeaWiFS processing. SeaWiFS Postlaunch Technical Report Series.

Rouault, M. and J. R. E. Lutjeharms. 2003. Estimation of sea-surface temperature around southern Africa from satellite-derived microwave observations. S. Afr. J. Sci. *99,* 489–494.

Saji, H. H., B. N. Goswami, P. N. Vinayachandran and T. Yamagata. 1999. A dipole mode in the tropical Indian Ocean. Nature, *401,* 360–363.

Schouten, M. W., W. P. M. de Ruitjer, P. J. van Leeuwen and H. A. Dijkstra. 2002. An oceanic teleconnection between the equatorial and southern Indian Ocean. Geophys. Res. Lett., *29* (16), 10.1029/2001GL014542.

Shapiro, R. 1970. Smoothing, filtering, and boundary effects. Rev. of Geophys., *8,* 359–387.

Torrence, C. and G. P. Compo. 1998. A practical guide to wavelet analysis. Bull. Amer. Met. Soc., *79,* 61–78.

Weeks, S. J. and F. A. Shillington. 1994. Interannual scales of variation of pigment concentrations from coastal zone colour scanner data in the Benguela upwelling system and the subtropical convergence zone south of Africa. J. Geophys. Res., *99,* 7385–7399.

—— 1996. Phytoplankton pigment distribution and frontal structure in the subtropical convergence region south of Africa. Deep-Sea Res. I, *43,* 739–768.

Weeks, S. J., F. A. Shillington and G. B. Brundrit. 1998. Seasonal and spatial SST variability in the Agulhas retroflection and Agulhas return current. Deep-Sea Res. I, *45,* 1611–1625.

Received: *12 September, 2003;* revised: *12 April, 2004.*